Biomedical Signal Processing and Control 51 (2019) 148–161

Contents lists available at ScienceDirect

Biomedical Signal Processing and Control

journal homepage: www.elsevier.com/locate/bspc

Automated Optic Disc region location from fundus images: Using local multi-level thresholding, best channel selection, and an Intensity Profile Model

Laura J. Uribe-Valencia*, Jorge F. Martínez-Carballido

Instituto Nacional de Astrofísica, Óptica y Electrónica, Tonantzintla, Puebla, Mexico

ARTICLE INFO

Article history:
Received 15 February 2018
Received in revised form
15 December 2018
Accepted 9 February 2019
Available online 27 February 2019

Keywords:
Optic disc
Color fundus image
Medical image analysis
Diabetic retinopathy

ABSTRACT

Background and objective: Location of optic disc, which corresponds to the visible part of the optic nerve in the eye, is of high importance for bright lesion detection of Diabetic Retinopathy by extracting it and avoiding false positives. Glaucoma detection processes details on the optic disc zone. Location of the macula uses optic disc location as a reference. Thus, the location of optic disc is relevant for several diagnosis procedures on retinal images. Several methods for OD detection in fundus images can be found in the literature; however, the issue is still open to reach better results in terms of accuracy, robustness and complexity. This work provides a simple and image resolution independent method for Optic Disc location for methods that use the optic disc zone elimination or extraction to perform some diagnosis.
Methods: This work proposes a simple and reliable method for OD region location in fundus images using four known publicity available datasets: DRIVE, DIARETDB1, DIARETDB0 and e-ophtha-EX. We are introducing an OD region location method based on OD's characteristic high intensity and a novel method for feature's extraction that aims to represent the essential elements that define an optic disc by proposing a model for the pixel intensity variations across the optic disc (column wise). The approach has four main stages: OD pixel region candidate generation, promising OD regions detection, promising candidate features extraction, and classification. All images from the four datasets were used for testing, since no training was used for classification.
Results: An OD location accuracy of 99.7% is obtained for the 341 retinal images within the four publicly datasets.
Conclusions: The obtained results show that the proposed method is robust and achieves the maximum detection rate in all four compared databases, which demonstrates its effectiveness and suitability to be integrated into a complete prescreening system for early diagnosis of retinal diseases. Use of promising OD region location reduces processing area in about 40%.

1. Introduction

Morphological detection of retinal structures such as the optic disc (OD), blood vessels, macula and fovea are a common step in most systems for automatic detection and screening of different retinal pathologies. Fundus images are used for diagnosis by trained clinicians to check for any abnormalities or changes in the retina. To alleviate physician work, images can be processed by an automated system that provides probable lesion areas, that the ophthalmologists will diagnose [1]. In particular, the detection of the OD, which corresponds to the visible part of the optic nerve in the eye, is an important task in retinal image analysis because it is a key reference for recognition algorithms [2], blood vessels segmentation [3,4], and diagnosing some diseases such as diabetic retinopathy (DR) [5,6] and for registering changes within the optic disc region due to diseases such as glaucoma [7–9] and the development of new blood vessels [10]. The OD is also a landmark for other retinal features, such as the distance between the OD and the fovea [11,12], which is often used for estimating the location of the macula [13] and is also used as a reference length for measuring distances in retinal images [14]. In addition, it is important to detect and isolate OD region because, most of the algorithms designed to segment/detect abnormalities such as hard exudates in DR will detect lots of false positives in OD region since the optic disc could present similar color, shape and size characteristics which can lead to potentially

* Corresponding author at: Instituto Nacional de Astrofísica, Óptica y Electrónica, Luis Enrique Erro # 1, Santa María Tonantzintla, Puebla, Pue. 72840 Mexico.
E-mail addresses: lauraj.uribe@inaoep.mx (L.J. Uribe-Valencia), jmc@inaoep.mx (J.F. Martínez-Carballido).

https://doi.org/10.1016/j.bspc.2019.02.006
1746-8094/

detect OD sections as exudates, negatively affecting the performance of the system [15]. Accurate identification of OD can be used to reduce the false positive rate while detecting the bright lesions [16].

Even though there is a significant variation in optic disc's appearance and size, it's mean diameter is clinically estimated on 1.5 mm [17] (near $(1/30)^{th}$ the of retina's area) and exhibits a distinctive appearance from the tissue zone that surrounds it due to the absence of pigment epithelium making OD's color paler than its surroundings. In healthy fundus images, optic disc is usually seen as a bright circular or elliptic region crossed by a tree of vesins and arteries [18]. Although the OD main features and characteristics are relatively easy to describe, individual differences, diseases and other factors will influence characteristics of the optic disc. There are several factors that difficult the correct OD detection, for example, in some of the images the edges of the OD are not clearly visible, and some OD regions can be obscured due to the blood vessels that pass through it. Image quality can also affect the appearance of the OD. A retinal image may be unevenly illuminated or poorly focused, resulting in a less distinct and/or blurred OD. On the other hand, when there is presence of injuries such as exudates or severe problems in the lighting; the pixels that present the highest values of intensity in the image do not always correspond to the optic disc. Optic disc location methodology involves extensive research interest [19,20], due to its relevance for OD diseases and as an anatomic eye's feature.

This work proposes a simple and reliable method for OD region location in fundus images. To make optic disc location robust, OD's characteristic high intensity is combined with a model of the profile pixel intensity variation. The approach comprises four main stages: OD pixel region candidate generation, promising OD regions detection, promising candidate features extraction, and classification. The proposed method consists on a top-down approach, namely, we go from a group of high intensity local regions with coarse level features to finer features on extended regions with minimum requirements on size and intensity distribution. The main contribution of this work can be summarized in five aspects: (1) About 40% of fundus image reduction is achieved by defining a promising region to locate the OD. (2) Unlike most approaches, both channels red and green are considered. The channel who exhibits the best range for candidate generation is selected for further processing. (3) No training is required, so all the images of the datasets are used for testing and no additional datasets are needed to train a classifier. (4) A novel method for feature's extraction is proposed, it aims to represent the essential elements that define an optic disc by proposing a model for the pixel intensity variations across the optic disc (column wise). (5) Since anatomical features calculated are relative to image's original resolution, the results of the proposed approach were achieved without any alteration on the original size of the input images, ensuring that our detection algorithm is applicable to any image resolution available in fundus image datasets. The approach's results proved to be reliable; especially for challenging images, including images with poor illumination, pathological changes, with dark OD due to uneven illumination and low contrast and images with bright exudates whose size and intensity are like OD. The proposed algorithm was tested in four publicly-available datasets achieving a competitive performance respect to other state-of-the-art methods.

The rest of the paper is organized as follows: in Section 2 the relevant and recent related work in detection of OD on fundus images is reviewed. In Section 3 the main stages of the proposed approach are described. In section 4 the characteristics of the public databases used are detailed. Section 5 shows the experimental results, the validation obtained using public databases, and a comparison with other methods from the literature. Finally, Section 6 provides the discussion and conclusions.

2. Related work

The optic disc detection approaches can be categorized in three groups: property-based methods, convergence of blood vessels and model-based methods; and a fourth group by combination of two or more of the first three.

2.1. Property-based methods

Property-based methods are based directly on the properties of the optic disc (e.g. location, size, color and shape). Rahebi & Hardalac [21] implemented a firefly algorithm to detect the optic disc in retinal fundus images. This algorithm was initially introduced at Cambridge University by Yang in 2008 [22]. The population in this algorithm includes the fireflies, each of which has a specific rate of lighting or fitness. In this method, the insects are compared two by two, and the less attractive insects can be observed to move toward the more attractive insects. Finally, one of the insects is selected as the most attractive, and this insect presents the best response of the available solutions to the problem in question. The light intensity of retinal image pixels is used as the firefly lightings. The movement of these insects due to local fluctuations produces different light intensity values in the images.

2.2. Convergence of blood vessels methods

Convergence of blood vessels approaches are based on the detection of optic disc by using the information provided by the vascular structure of the retina, since the optic nerve is the focal point of the retina's blood vessel network [23]. To locate the optic disc by this method, the retinal blood vessel network is first detected. Soares et al. [24] proposed an algorithm with a new vessel enhancement method based on a modified corner detector. A weighted version of the vessel enhancement is combined with morphological operators, to detect the four main vessels orientations $\{0^\circ, 45^\circ, 90^\circ, 135^\circ\}$. These four image functions determine an initial optic disc localization, resulting in two images vertical or horizontal orientations. Each division is averaged creating a 2D step function, and a cumulative sum of the different sizes step functions is calculated in the 2 orientations, resulting in an initial optic disc position. The final OD is determined by a vessel convergence algorithm using its two most relevant features; high vasculature convergence and high intensity values.

Wu et al. [25] presented a novel method to automatically localize ODs in retinal fundus images based on directional models. According to the characteristics of retina vessel networks, such as their origin at the OD and parabolic shape of the main vessels, a global directional model, named the relaxed bi-parabola directional model (R-BPDM), is first built. The main vessels are modelled by using two parabolas with a shared vertex and different parameters. A local directional model, named the disc directional model (DDM), is built to characterize the local vessel convergence in the OD as well as the shape and the brightness of the OD. Finally, the global and the local directional models are integrated to form a hybrid directional model, which can exploit the advantages of the global and local models for highly accurate OD localization.

Panda el al. [26] proposed a robust approach for OD localization, incorporating three salient visual cues derived from retinal vasculature symmetry and convergence characteristics, namely (1) global vessel symmetry, (2) vessel component count and (3) local vessel symmetry inside OD region. The initial OD center location is computed using the highest number of major blood vessel components in the skeleton image and the final OD center localization involves an iterative center of mass computation to exploit the local vessel symmetry in the OD region of interest.

Roychowdhury et al. [27] proposed a classification-based optic disc (OD) segmentation algorithm that detects the OD boundary

and the location of vessel origin (VO) pixel. First, the green plane of each fundus image is resized and morphologically reconstructed using a circular structuring element. Next, the bright regions of the reconstructed image that lie in close vicinity of the major blood vessels are selected and later classified as bright probable OD regions and non-OD regions using six region-based features and a Gaussian mixture model classifier and finally, the centroid of major blood vessels within the segmented OD boundary is detected as the VO pixel location.

2.3. Model based methods

The model-based methods rely in the fact that optic disc shape is approximately circular and that the pixels conforming its area are brighter than its surroundings. The method consists on comparing a template image (model) with a group of candidates in the fundus image, with the purpose to determine the candidate that exhibits the best match. The created template is applied as a running window of NxN size along the fundus image and the correlation between the template and the section of the image is calculated, the region with the highest correlation is selected as the OD region. Wang et al. [28] used a template matching method to approximately locate the optic disc center, and the blood vessel is extracted to reset the center. This is followed by applying the Level Set Method, which incorporates edge term, distance-regularization term and shape-prior term, to segment the shape of the optic disc.

2.4. Combination of methods

Combination of methods group correspond to those OD detection methods that don't rely only on the OD's properties, convergence of vessels or matching a template. Instead they combine two or more of the above methods exposed. Harangi & Hajdu [29] stated that there's no reason to assume that any single algorithm would be optimal for the detection of various anatomical parts of the retina. It is difficult to determine which is the best approach, because good results were reported for healthy retinas but weaker ones for more challenging datasets containing diseased retinas with variable appearance of ODs in term of intensity, color, contour definition and so on. To overcome this, they studied and adapted some of the state-of-the-art OD detectors and finally organized them into an ensemble framework to combine their strengths and maximize the accuracy of the localization of the OD. Basit & Fraz [30] method for automatic detection of the optic disc locus and optic disc boundary extraction is proposed based on morphological operations, regional properties, and marker-controlled watershed transform. The claimed advantages over other methods are: it works well on a vast variety of illuminations present in retinal images, it only extracts the main blood vessels centerline from the image and the combination of extracted vessels centerline and local maxima make the proposed method more tolerant to error for the optic disc location. Xiong & Li [7] approach has three main steps: region-of-interest detection, candidate pixel detection, and confidence score calculation. The features of vessel direction, intensity, OD edges, and size of bright regions were extracted and employed in the proposed OD locating approach. Authors claim that compared with the methods using vessel edge information only, the improvement on candidate pixel detection and the confidence value achieves promising results in the following situations: the images with dark OD due to uneven illumination and low contrast; the retinal images with incomplete OD; the images with bright exudates, whose size and intensity are like OD.

In Bharkad [31] proposed method, an equiripple low pass finite impulse response (FIR) filter was designed to suppress the dominance of blood vessels and to enhance the OD region. The specifications of the equiripple low pass filter were empirically obtained. Then the brightest pixel having maximum intensity among all pixels of low pass filtered image of retina is found. A Threshold is computed by considering the mean intensity of square region of pixels around the brightest pixel. The OD is located by determining the circular shape small cluster of high intensity pixels using compactness property of circular region. For segmentation of the OD region, square portion approximately twice the OD size in green component of retinal image around the OD center is cropped. Finally, a morphological dilation operation with a disc structuring element of radius half the actual size of the OD is performed to enhance the bright region of the OD.

Rodrigues et al. [32] proposed an algorithm built on wavelets transforms and mathematical morphology for detecting the OD. The OD is processed in a gray level image selected by a histogram analysis that consists on comparing the color bands with three reference images. The band to process is selected based on the highest level of histogram similarity of the input image with an image reference. Next, to enhance the bright region of the OD, the calculated best band is submitted to an enhancement by a white top hat, using a circular structuring element with radius 25. Finally, the image is submitted to a pyramidal "Haar" wavelet decomposition that produces a sub band vector containing the image approximation frequencies.

Chakravarty et al. [33] proposed method includes a first rough Region of Interest (ROI) extraction by employing a simple image processing method based on intensity thresholding and Hough Transform. Also, they proposed a novel boundary-based Conditional Random Field formulation that extracts both the optic disc and cup boundaries in a single optimization step. Optic disc depth was modelled with estimations from the fundus image itself using a coupled, sparse dictionary trained on a set of image-depth map.

3. Methodology

The optic disc can be characterized as a bright, yellowish, circular region in a retinal image. On healthy fundus images, these characteristics remain and pixels with the highest values of intensity correspond to the optic disc. However, on abnormal fundus images with presence of large clusters of exudates and severe illumination artifacts, optic disc location based only on intensity information is unreliable. To make optic disc location robust and reliable, intensity information can be combined with information derived from the blood vessels, given that the optic disc is the entry point of the entire vessel network. In this section, an approach for OD location in retinal images based on high intensity information combined with a column wise model of the profile pixel intensity variation is proposed. The method comprises four main stages: OD pixel region candidate generation, promising OD regions detection, promising candidate features extraction, and classification. Fig. 1 gives the methodology overview. The notations and their definitions used in this OD location methodology, are defined in Table 1.

3.1. OD pixel candidate generation

The purpose of this stage is to obtain all the locally high intensity regions present in the image, to ensure promising OD locations on the whole image are extracted to subsequent processing stages. The generation of these regions take four steps: (1) preprocessing, (2) region-of-interest mask generation, (3) contrast enhancement and (4) image partitioning and local thresholding. Table 2 describes the steps of the algorithm to generate the OD pixel candidate.

3.1.1. Preprocessing

Fundus images taken at standard exams are prone to contain noise and low contrast, and in addition with the non-uniform illumination produce retinal images with poor quality. Therefore, surging the need for preprocessing these images, for an appropri-

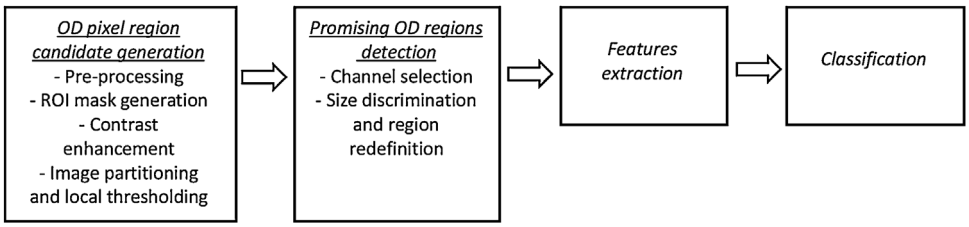

Fig. 1. Overview of the proposed methodology for optic disc region location, this 4-step process is applied to each fundus image.

Table 1
Definition of notation.

Notation	Meaning
ROI	Region-of-interest
ImgC	Image containing potential OD regions
c_0	Start column of the ROI rectangle
c_1	Final column of the ROI rectangle
Diam	OD diameter approximate value
CLAHE	Adaptive enhancement of the histogram with limited contrast
Img_{ODcand}	OD promising candidate regions
winR	horizontal band based on OD's diameter
chx	Color channel with the best contrast according to *ic* index
avgChx	Mean value of the profile consisting of the maximum intensity values per column on *chx* channel.
LB	Left-Background
LL	Left-Lobe
V	Vasculature
RL	Right Lobe
RB	Right Background
Sf	Scale factor
SLIC	Simple linear iterative clustering
Imgspxls	Image of superpixel segmentation of the candidate image region where each superpixel region value is set to its mode value
Diff_Profile	Profile derived from the difference per column of the maximum intensity values with a moving mean filter with a size of the expected vein diameter applied to its differences profile.

Table 2
Algorithm to generate the OD pixel candidate.

Algorithm 1: Candidates generation
input : Original image of dataset (DRIVE, Diaretdb0, Diaretdb1, e-ophtha)
output : Image containing potential OD regions (ImgC)

```
Preprocess image to homogenize areas (noise reduction)
Mask out left and right dark region of the image
Redefine initial and final column excluding masked region
Determine OD's Diameter estimate
Enhance contrast of the green channel
Use one horizontal and three vertical bands for most probable OD location
Begin
for each vertical band
    Use 3 threshold bands from maximum to mode pix value
        Generate a RGB (ImgC) for the three bands
            Red is high threshold band
            Green is medium threshold band
            Blue is low threshold band
    end
End
```

ate automated clinical diagnosis. A median 3×3 filter is applied to reduce image noise. The effect of the attenuation of the edges in an image generated by the smoothing effect of linear filters, such as that of the average filter, is generally undesired, the filter of the median allows to eliminate artifacts and unwanted structures in the image without significantly affecting the edges. The main function of the median filter is to force points with very different intensity values to their neighbors to have values closer to them, in this way the intensity peaks that appear in isolated areas are eliminated.

Fig. 2. Original fundus image.

Median filter operates replacing the value of a pixel f(x,y) with the median of all of the pixels in the neighborhood of that pixel as shown in Eq. (1).

$$f_{med}(x,y) = median\ \{f(s,t)\},\ sz\ \in I\,odd\,and\,greater\ than\,1,$$
$$s = \left\{x - \frac{sz-1}{2}\ to\ x + \frac{sz-1}{2}\right\}\ and\ s \neq x,$$
$$t = \left\{y - \frac{sz-1}{2}\ to\ y + \frac{sz-1}{2}\right\}\ and\ t \neq y \tag{1}$$

3.1.2. Region-of-interest (ROI) rectangle

Fundus image is composed by a central semi-circular region of interest (the fundus of an eye) and dark zones surrounding it. A Mask is created with the purpose to exclude the left and right dark areas of eye fundus for further processing, saving computing time and reducing possibility of noise. The semi-circular foreground region is referred as ROI. The mask image is a binary image where the ROI pixels are set to one and the background pixels to zero. On Fig. 3 the stages for ROI rectangle extraction are shown applied on the original fundus image on Fig. 2. ROI rectangle for the original image is generated as follows:

- Eliminate dark noise from channels Red and Green by thresholding pixel intesity above 10 both channels and multiplying by Red channel. Next, a range filter with a 15×15 window is applied. The range filter is defined by Eq. (2).

$$Range(A(x,y)) = \max[A(x+i,\ y+j)] - \min[A(x+i,\ y+j)],$$
$$where\,i,j\ \in\ \left(-\frac{sz-1}{2}\ to\ \frac{sz-1}{2}\right),\ sz\ \in I\,odd\,and\,greater\ than\,1 \tag{2}$$

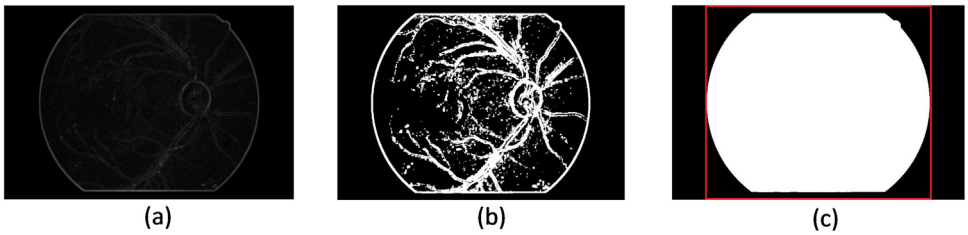

Fig. 3. (a) Result of applying a range filter with a 15×15 window. (b) Result of applying a threshold of the highest 20 percent of image (a). (c) Region-of-interest (ROI) rectangle (red).

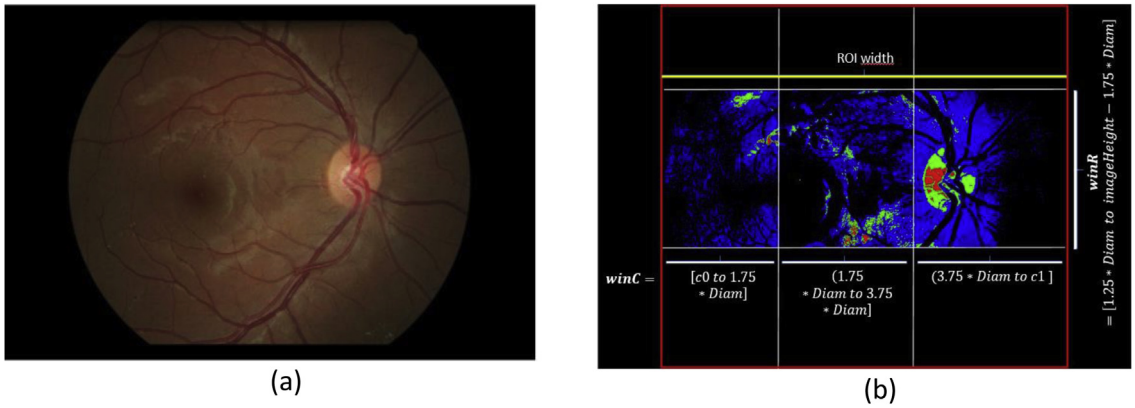

Fig. 4. (a) Original fundus image (b) Image partitioning and local thresholding. $\text{Img}_{\text{ODcand}}$ is the set of all red sub-regions.

- Threshold for the highest 20 percent, make a column pixel value sum, and find peaks higher than one fifth of the image height. Take column position for first and last peaks adjusted for the window size on the range filter. These being our start 'c_0', and end 'c_1' column for the ROI rectangle. As for the row range, the 70 percent central band is selected, given that no OD will be at top or bottom 15 percent. As given in Eq. (3)

$$ROI_{width} = c0 - c1 + 1 \tag{3}$$

$$OD\ diameter\ \ approximate\ \ value\ as\ Diam = \frac{ROI_{width}}{6}$$

3.1.3. Contrast enhancement

Eye images are commonly taken at non-uniform lighting environments, in addition, illumination diminishes as distance of a region from the center of the image increases. In the literature, there is a great variety of methods for improving contrast, aiming to increase the level of differentiation of the characteristics of the retina. Conventional methods based on the global histogram of the image such as contrast stretching and histogram equalization tend to result in loss of information in the brightest areas as well as in the dark areas of the background image, which is why adaptive enhancement of the histogram with limited contrast (CLAHE) [34] is commonly used. This technique operates in small regions of the image, improving the contrast by local equalization of the histogram, whereby small regions of interest are highlighted throughout the image. To enhance contrast of the fundus image, CLAHE is applied to the green channel of the ROI rectangle.

3.1.4. Image partitioning and local thresholding

Due to the non-uniform illumination, local intensity variations are found along the fundus image making unreliable the use of a global high intensity threshold to locate promising OD regions. To overcome this, the fundus image is partitioned into windows or sub-images for the extraction of local OD candidate regions. As OD diameter is estimated using the ROI, one horizontal band and three vertical bands are defined based on OD's diameter. A threshold for each of the three defined sub-regions is calculated, based on the maximum and the mode intensity value. Using the green channel, the partitioning and local threshold are defined as:

$$Horizontal\ \ band : \boldsymbol{winR} = [1.25 * Diam\ to\ imageHeight - 1.75 * Diam]$$

$$Vertical\ bands : \boldsymbol{winC} = \Big\{ [c0\ to\ 1.75 * Diam],\ (1.75 * Diam\ \ to\ 3.75 * Diam],\ (3.75 * Diam\ to\ c1\ ] \Big\}$$

$$\boldsymbol{delta} = \frac{window\ \max\ value - window\ \ mode\ value}{4.75}$$

$$\boldsymbol{threshold} = window\ \max\ value - delta \tag{4}$$

For each window, pixels higher than the local *threshold* are considered as relevant OD regions, and altogether conform the OD promising candidate regions ($\text{Img}_{\text{ODcand}}$). Fig. 4 illustrates the partitioning of promising region along with their local thresholding.

3.2. Promising OD regions detection

Once all the relevant local high intensity regions are extracted, more detailed features select most promising ones. The approach consists in going from a group of regions with coarse level features to finer features on extended regions with minimum requirements on size and intensity distribution. Next, the steps of this proposal to select regions with better characteristics to contain an OD:

3.2.1. Channel selection

The channel with better contrast between green and red is selected for posterior processing. First, two subsections of the image are defined, horizontal band is defined by *winR,* vertical left

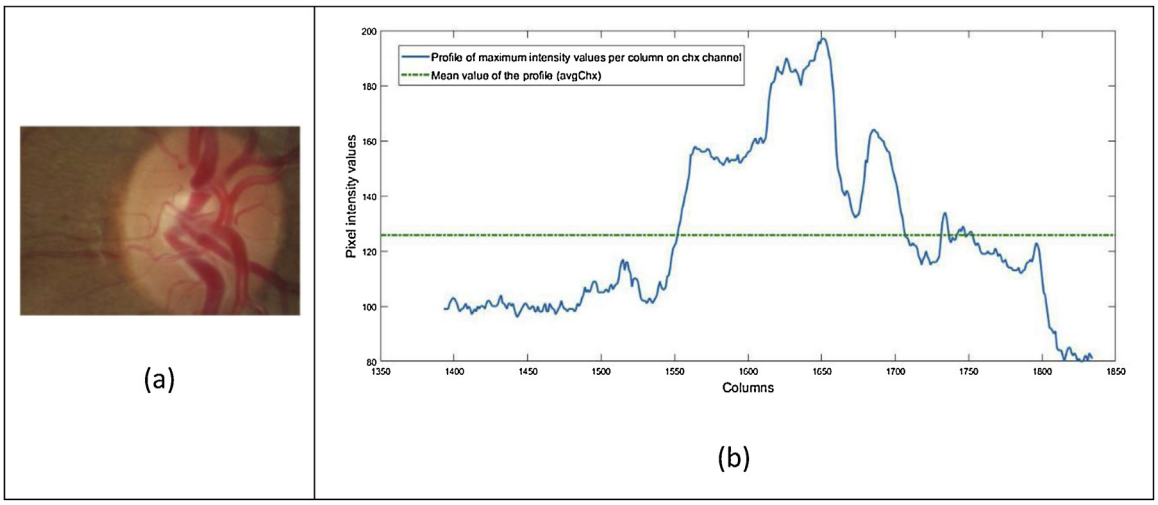

Fig. 5. a) OD candidate region (b) Profile of the maximum intensity values per column on chx channel for image (a).

band is given by ([$c0\,to\,2.750 * Diam$] and vertical right band by [$3 * Diam\,to\,c1$].

A median filter of size 7×7 is applied to both channels. An index $ic = \frac{maximum\ intensity\ value - mode\ value}{mode\ value}$ for both channels on left and right bands, resulting in four *ic* index values, the higher *ic* gives the channel and vertical band with more intensity variation (*chx, side*) on the intensity range of interest as previously determined by the relevant regions. *side* of *chx* with better contrast will be further considered.

3.2.2. Size discrimination and region redefinition

- Given Img_{ODcand}: regions must be between height and width greater than (1/20)**Diam*, and height and width less than *Diam*.
- Regions are centered and extended. The center is given by using the '*WeightedCentroid*' concept, which considers pixel intensities in the image region as weights in the centroid calculation, intensities used are defined by the yellowish proportion of pixels in the region. Then, the region is extended around the centroid coordinates by half of *Diam*, *ROIcentroid*. Next, a threshold value is calculated using *chx* channel for the *ROIcentroid*:

$$diff = (maximum\ value - mode\ value)$$

$$delta = \begin{cases} \frac{dif}{4.75}, & if\ \ diff > 30 \\ 6 & if\ diff \leq 30 \end{cases}$$

$$Threshold_e = maximum\ \ value - 3 * delta$$

- Apply $Threshold_e$ to the *ROIcentroid*, resulting regions are filtered to be: Region_width greater than *Diam*/10 and Region_height greater than *Diam*/8.
- These remaining regions are extended again, this time width is increased by *Diam*/9 on each side and height by *Diam*/2 at the top and bottom.
- A profile consisting of the maximum intensity values per column on *chx* channel is calculated for the remaining extended regions, mean value of this profile is defined as *avgChx*. Fig. 5. (a) gives a candidate region and (b) shows its profile of the maximum intensity values per column.
- Promising OD regions are selected if prominences above *avgChx* have width higher than *Diam*/10.

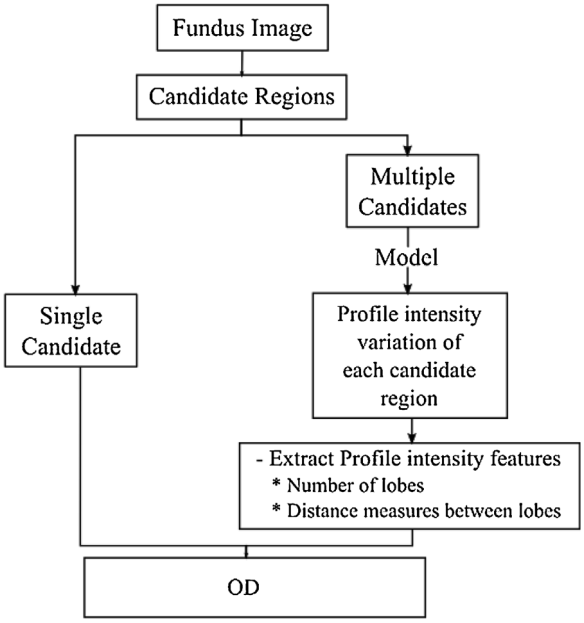

Fig. 6. Overview of the proposed steps for feature's extraction.

3.3. Features extraction

The purpose of this stage is to calculate a set of features for all the regions labeled as promising OD regions from the previous stage. Feature's extraction step is applied for cases where there is more than one candidate OD region on a fundus image as detailed in Fig. 6.

The proposed method for feature's extraction aims to represent the essential elements that define an optic disc by modelling the pixel intensity variations across the optic disc (column-wise). On an ideal fundus image quality and illumination conditions, OD's column-wise intensity change behavior could be seen as an stable left-background zone followed by the border of the first bright OD section, where the intensity difference will be positive growing, next change in intensity difference will be expected when the vasculature is reached, where is expected that the intensity difference will negatively grow until the limit of the second bright OD section is reached, in this point again the intensity difference will be positive growing until the OD border is reached where the intensity difference will negatively grow until the right-background zone is reached where the intensity difference will be stable again.

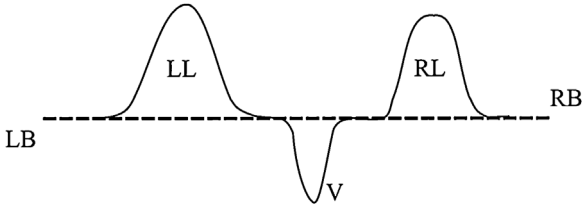

Fig. 7. Profile pixel intensity variation column wise model of an ideal OD.

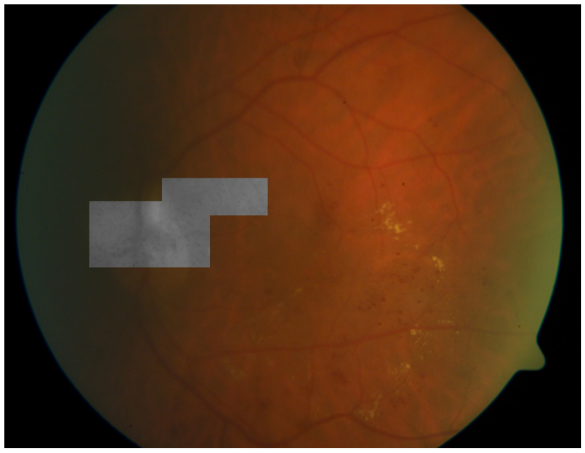

Fig. 8. Candidate image regions marked on gray (image020.png from Diaretdb0 dataset).

Modelling this column wise pixel intensity variation of an optic disc as depicted in Fig. 7 where we highlight the five change sections previously described as LB-LL-V-RL-RB. These five sections and their distances will be the set of features to distinguish between the OD and the other candidate regions.

Where: Left-Background (*LB*), Left-Lobe (*LL*), Vasculature (*V*), Right Lobe (*RL*) and Right Background is (*RB*).

The steps used to model the column-wise pixel intensity variation profile (Fig. 7) are the following:

- Pre-processing candidate regions.
- Redefining possible OD pixel region.
- Candidate image regions segmentation using Superpixels.
- Calculate column-wise pixel intensity variation profile.

3.3.1. *Pre-processing candidate regions*

In order to highlight the veins, a minimum filter with window size of 7 is applied to the green channel of each candidate region, then to improve region contrast, a scale factor (*sf*) is applied. *sf* is calculated as:

$$sf = \frac{255}{Maximum\,pixel\,value\,on\,the\,candidate\ \ region}$$

The scaled region candidate is then obtained multiplying the region by sf. Pre-process steps for candidate OD regions of image020.png from Diaretdb0 dataset (Fig. 8) are illustrated on Fig. 9.

3.3.2. *Redefining possible OD pixel region*

In general, we observed that candidate OD regions often contain large zones of background and undesired artifacts due to low quality and the non-uniform illumination. Knowing that borders can be seen as high intensity changes in contiguous pixel positions and aiming to redefine a region whose column limits correspond to the OD borders, we calculated for each pre-processed candidate region (Fig. 9(c)), the profile of maximum pixel intensity values per column (Fig. 10. blue) and its difference per columns (Fig. 10. red). The highest difference values define what is expected to be the OD borders (positive for left-border) and negative for veins and right-border positions (Fig. 10. yellow). The new limits for the columns of the candidate regions are defined by the leftmost and rightmost positions of up to seven highest absolute differences considered as relevant (Fig. 11).

3.3.3. *Candidate image regions segmentation using Superpixels*

The concept of superpixel was first introduced by Xiaofeng Ren and Jitendra Malik in 2003 [35]. Superpixels segmentation aims to group connected pixels with similar gray levels to create visually meaningful pixel regions while heavily reducing the amount of data for subsequent processing steps. The clustering method selected for the superpixel segmentation was the simple linear iterative clustering (*SLIC*) algorithm [36] and the number of superpixels for each candidate image region is set to 15. Fig. 12(a) shows the result of applying the superpixel segmentation to a candidate region. The image in Fig. 12(b) correspond to set each pixel intensity value of a superpixel region to the value of the mode of the region, this new color representation of the superpixel regions has the intent of reduce intensity variability for the subsequent feature's extraction step.

3.3.4. *Column wise pixel intensity variation profile*

To represent the column wise pixel intensity variation, first, the maximum intensity value per column of *Imgspxls* Fig. 13(a) is calculated as depicted in Fig. 13(b). Next step is calculating the difference per column of the maximum intensity values as shown in Fig. 13(c) and finally, to soften details, a moving mean filter with a size of the expected vein diameter (OD radio/10) is applied to the differences profile Fig. 13(d). This final profile (*Diff_Profile*), will be the profile which will be compared with the profile pixel intensity variation column wise model of an ideal OD (Fig. 7) for optic disc candidate region classification.

3.4. *Feature's set and classification*

The pattern on *Diff_Profile* that defines an Optic disc region is the presence of a Left Lobe (LL), a Right Lobe (RL) and Vasculature (V) between them, the distances from LL to V and V to RL must correspond to approximately (2/3) OD diameter and (1/3) OD diameter in any order. A sample of this behavior in a true OD region candidate is depicted in Fig. 14(c).

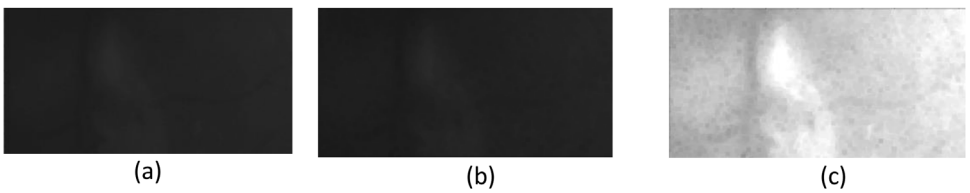

Fig. 9. (a) Original candidate image region. (b) Result of applying a minimum filter with a 7×7 window. (c) Result of scaling (b) by the sf factor.

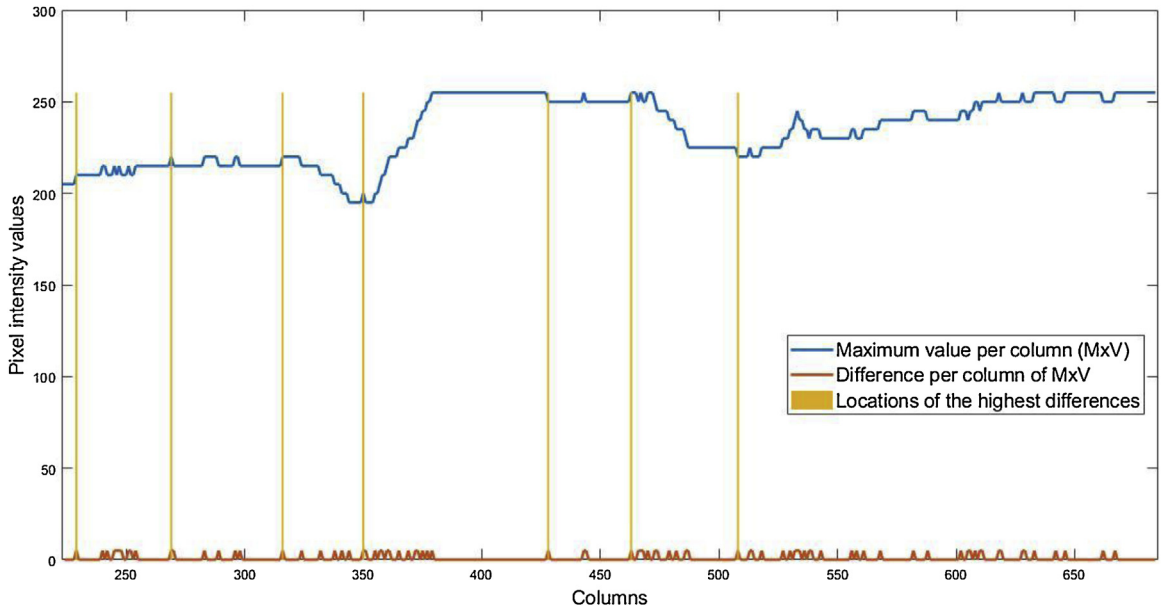

Fig. 10. Maximum pixel intensity values per column (blue), intensity difference per column (red), column locations of the highest difference values (yellow).

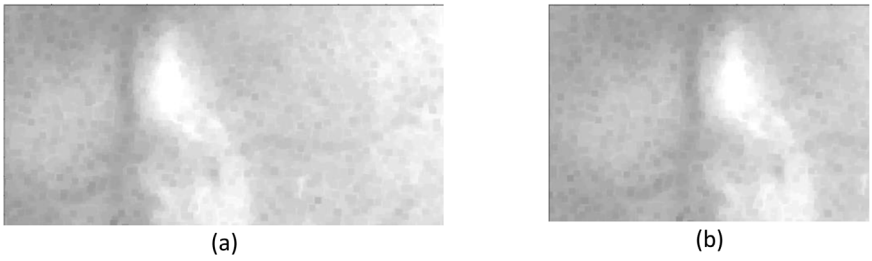

Fig. 11. (a) Pre-processed candidate image region. (b) Pre-processed candidate image region with redefined column limits.

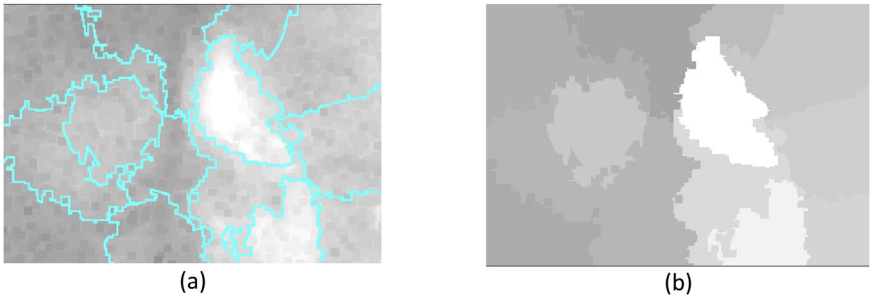

Fig. 12. (a) Superpixel segmentation of the candidate image region. (b) Each superpixel region value is set to its mode value (Imgspxls).

To illustrate the behavior on *Diff_Profile* for candidate regions which do not correspond to true OD regions, we selected examples for the 3 most common cases of OD region confusion: presence of reflections along the veins Fig. 15, zone of exudates and hemorrhages of considerable size Fig. 16 and presence of reflections on fundus image boundaries Fig. 17. In the 3 cases the *Diff_Profile* pattern LL-V-RL is not present.

4. Materials

With the purpose to evaluate and validate the proposed approach, four publicly available retinal image datasets were tested: DIARETDB1 [37], DIARETDB0 [38], e-ophtha-EX [39], and DRIVE [40]. Table 3 presents the characteristics for each dataset.

DIARETDB1 dataset contains 89 fundus images, where 84 of them have at least some signs of mild proliferative DR and five images are of a healthy retina. The images were marked by four experts for the presence of micro aneurysms, hemorrhages, and hard and soft exudates.

DIARETDB0 includes 130 color fundus images. Of these, 110 contain signs of DR (exudates, microaneurysms, hemorrhages or

Table 3
Description of the four publicly available retinal image datasets tested.

Dataset name	Dataset size	Image size (rows x cols)	#Healthy/Disease Images
DIARETDB0	130	1152 × 1500	20/110
DIARETDB1	89	1152 × 1500	5/84
DRIVE	40	565 × 584	33/7
E-OPHTHA-EX	82	1696 × 2544 1360 × 2048 960 × 1440 1000 × 1504	35/47

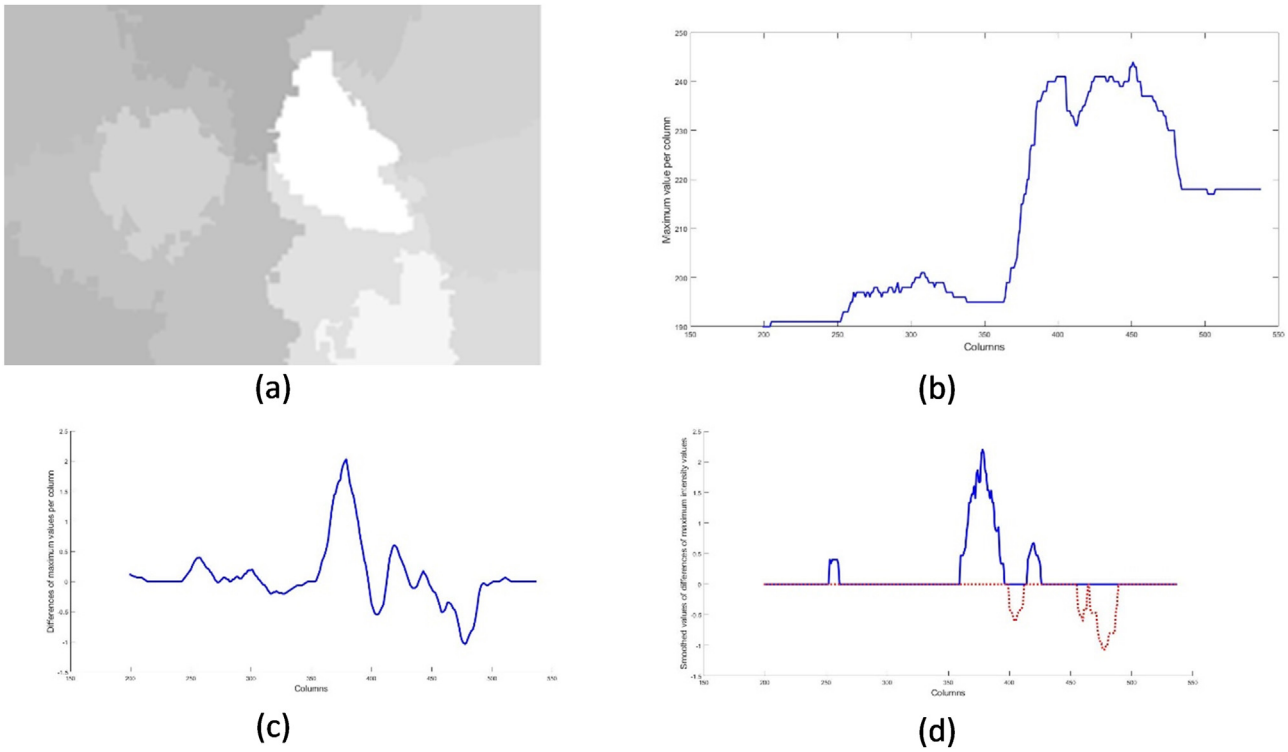

Fig. 13. (a) Imgspxls. (b) Maximum intensity value per column of Imgspxls. (c) Difference per column of the maximum intensity values (d) Diff_Profile, result of applying a moving mean filter with a size of the expected vein diameter (OD radio/10) to (c).

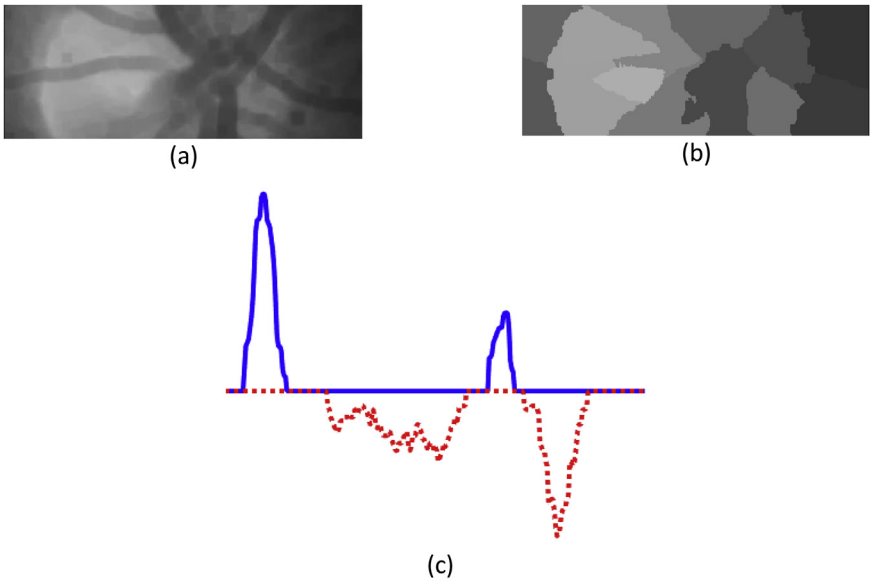

Fig. 14. (a) OD region candidate. (b) Imgspxls representation for OD region candidate. (c) Diff_Profile, showing the pattern LB-LL-V-RL-RB.

neovascularization) and 20 with healthy retina. Both datasets were taken with a 50 °FOV with a resolution of 1500 × 1152 pixel in PNG format.

The e-ophtha-EX dataset contains 82 fundus images, 47 images with exudates and 35 images with no lesion. This dataset was particularly designed for scientific research in diabetic retinopathy. Images have four different resolutions: 1696 × 2544, 1360 × 2048, 960 × 1440 and 1000 × 1504 pixels in JPG format.

DRIVE dataset contains 40 images, of them seven contain pathology. The photographs were obtained from a DR screening program in the Netherlands, using a Canon CR5 non-mydriatic 3CCD camera with a 45° field-of-view. The size of the images in this dataset is 584 × 565, and the images are in JPEG format.

The four datasets contain many challenging images, including: uneven illumination, bright artifacts, large areas of lesions such as exudates, hemorrhages, or drusens and circular scars left after Pan-Retinal Photocoagulation treatment (PRP).

Unlike the typical approaches, since no training is required, all the images of the four datasets are used for testing and no additional datasets are introduced to train a classifier. Also, there is no need to re-size the images, since anatomical features calculated are relative to image's original resolution.

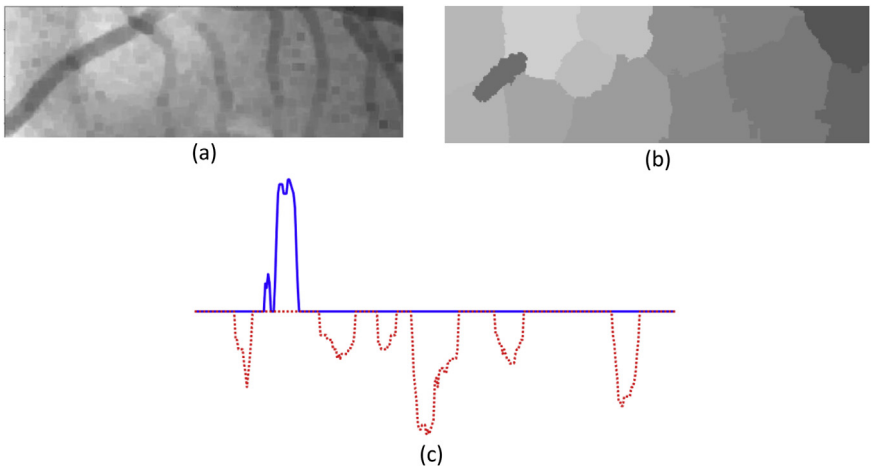

Fig. 15. (a) OD region candidate due to presence of reflections along the veins. (b) Imgspxls representation for OD region candidate. (c) Diff_Profile, where the pattern LL-V-RL is not present.

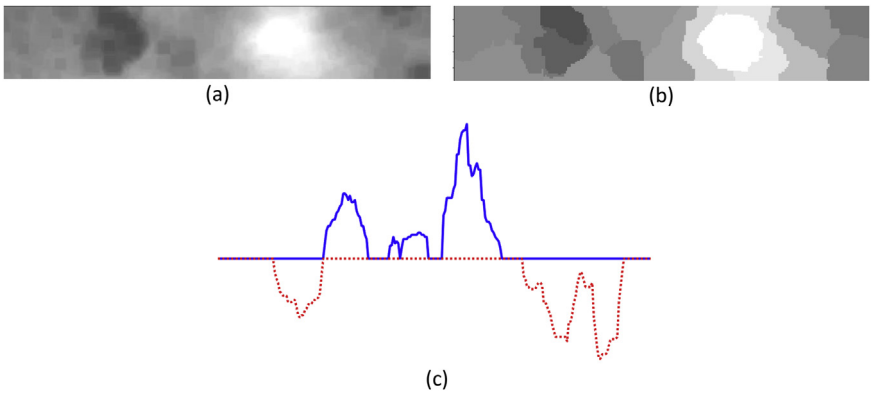

Fig. 16. (a) OD region candidate due to presence of zones of exudates and hemorrhages of considerable size. (b) Imgspxls representation for OD region candidate. (c) Diff_Profile, where the pattern LL-V-RL is not present.

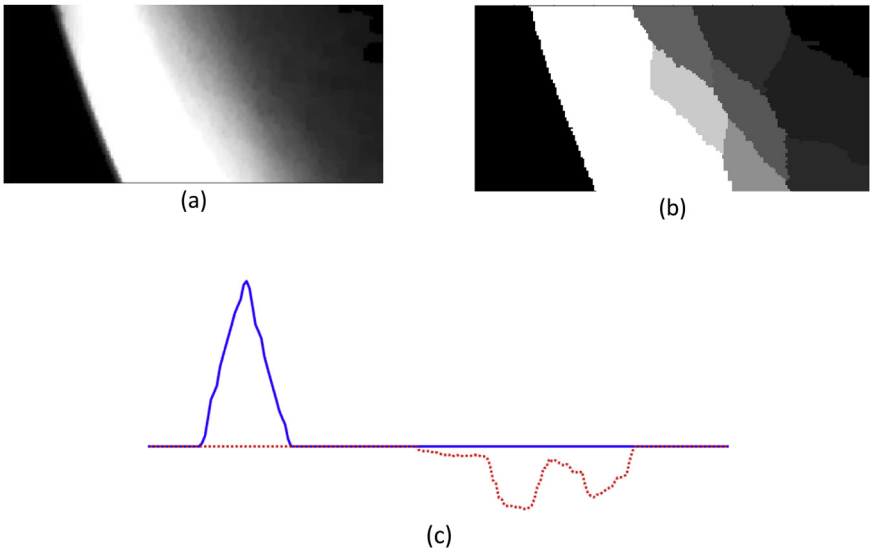

Fig. 17. (a) OD region candidate due to presence of reflections on fundus image boundaries. (b) Imgspxls representation for OD region candidate. (c) Diff_Profile, where the pattern LL-V-RL is not present.

Table 4
Comparison of OD detection success rates (expressed in %) in DIARETDB1, DIARETDB0, E-OPHTA and DRIVE public datasets.

Author	Dataset	Method type	#Images	OD success rate
Harangi et al. [29]	DIARETDB1	Combination of	89	(88/89) 98.88
	DIARETDB0	methods	130	(128/130) 98.46
	DRIVE		40	100
Basit et al. [30]	DIARETDB1	Combination of	89	(88/89) 98.88
	DRIVE	methods	40	100
Xiong et al. [7]	DIARETDB1	Combination of	89	(87/89) 97.75
	DIARETDB0	methods	130	99.23
	DRIVE		40	100
Soares et al. [24]	DIARETDB1	Convergence of blood	89	(88/89) 98.88
	DIARETDB0	vessels	130	(128/130) 98.46
	DRIVE		40	100
	e-ophtha-EX		82	(81/82) 98.78
Wu et al. [25]	DIARETDB1	Convergence of blood	89	100
Rahebi et al. [21]	DIARETDB0	vessels	130	100
Wang et al. [28]	DRIVE	Property-based	40	100
Bharkad [31]	DIARETDB1	Model-based	89	(84/89) 94.38
Rodrigues et al. [32]	DRIVE	Combination of	40	100
Panda et al. [26]	DIARETDB1	methods	89	(87/89) 97.75
	DIARETDB0	Combination of	130	(127/130) 97.69
	DRIVE	methods	40	100
	DIARETDB1	Convergence of blood	89	(88/89) 98.88
	DIARETDB0	vessels	130	(126/130) 96.92
	DRIVE		40	100
	DRIVE		20	(19/40)
	DIARETDB1		89	(19/20) 95
	DIARETDB0		130	100
	DRIVE		40	(126/130) 96.92
	e-ophtha-EX		82	100
				100
Proposed method	DIARETDB1	**Combination of**	**89**	**(89/89) 100**
	DIARETDB0	**methods**	**130**	**(130/130) 100**
	e-ophtha-EX		**82**	**(81/82) 98.78**
	DRIVE		**40**	**(40/40) 100**

5. Results and discussion

Four publicly available datasets were used: DIARETDB1 [37], DIARETDB0 [38], e-ophtha-EX [39] and DRIVE [40]. The algorithm for the proposed method was implemented with MATLAB R2017a in a laptop with Windows 10, 8 GB of RAM, and Intel i7 processor at 2.3 GHz.

Table 4. presents, the optic disc detection results for the 4 experimented datasets. Figs. 19–22 show some examples of the detected OD from each dataset, including the most challenging images that include pathologies, bright artifacts, or OD in dark area. The white rectangle shows the detected optic disc location for each image. When the white rectangle intersects the marked OD area it is considered as a correct location .

An OD location accuracy of 99.7% is obtained for the 341 retinal images within the four publicly datasets. Comparing with work from [25,24] which are recent methods found in the literature

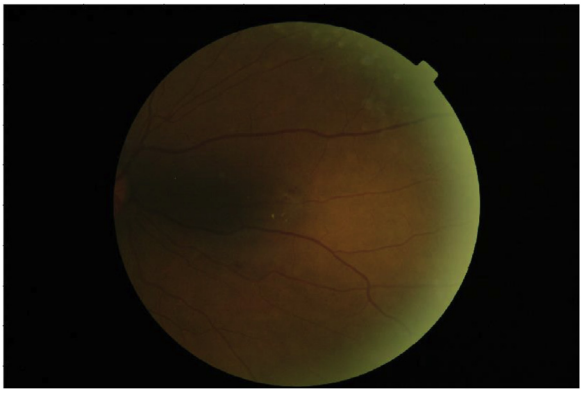

Fig. 18. Case where proposed method fails to detect OD. Image DS000F4K.jpg from e-ophtha-EX dataset.

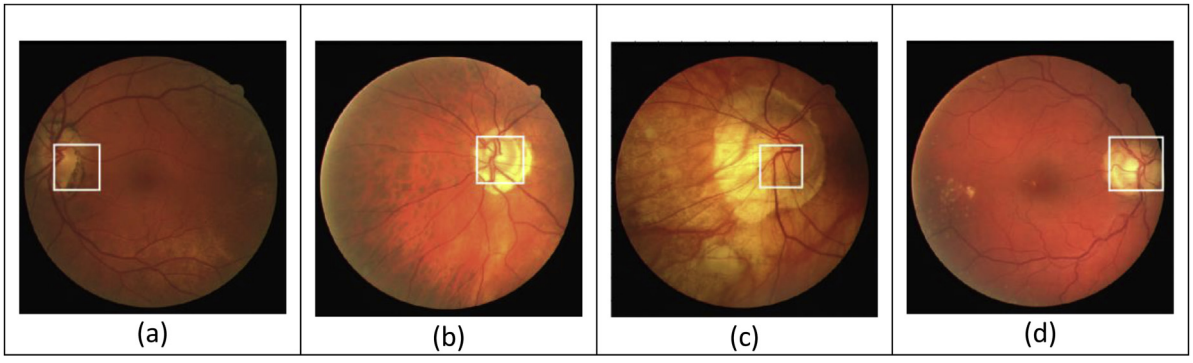

Fig. 19. Some results of OD localization on DRIVE dataset (white rectangle represents the OD region detected). (a) 26_training.tif (b) 31_training.tif (c) 34_training.tif (d) 08_test.tif.

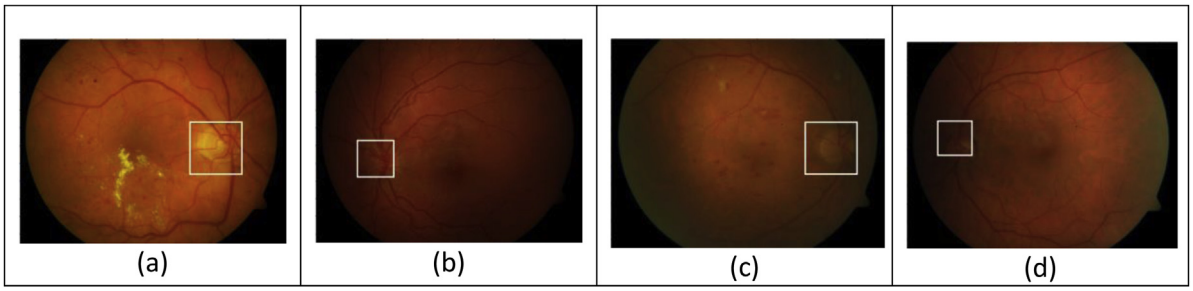

Fig. 20. Some results of OD localization on Diaretdb1 dataset (white rectangle represents the OD region detected). (a) diaretdb1_image019.png (b) diaretdb1_image087.png (c) diaretdb1_image064.png (d) diaretdb1_image059.png.

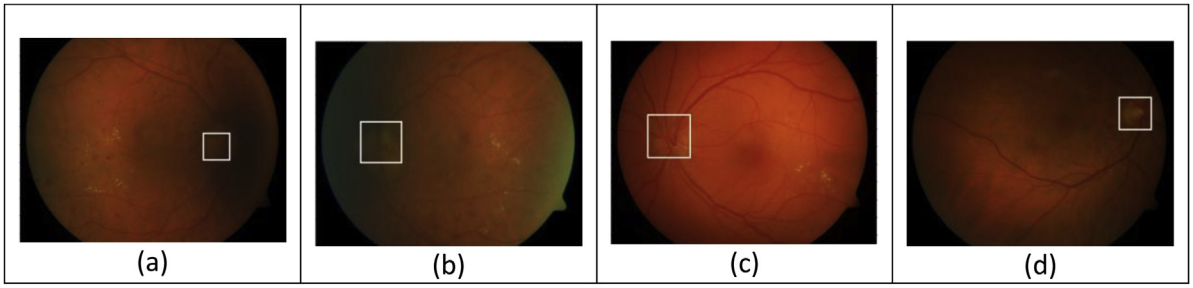

Fig. 21. Some results of OD localization on Diaretdb0 dataset (white rectangle represents the OD region detected). (a) image019.png (b) image020.png (c) image030.png (d) image117.png.

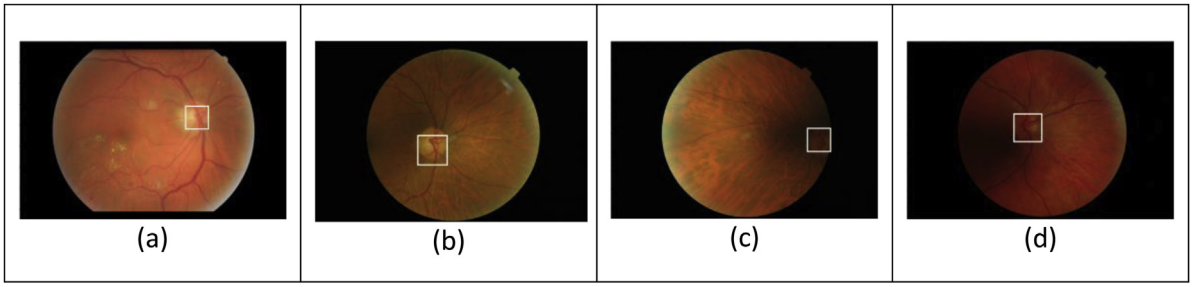

Fig. 22. Some results of OD localization on e-ophtha-EX dataset (white rectangle represents the OD region detected). (a) C0024407.jpg (b) DS000DGV.jpg (c) DS000DGZ.jpg (d) DS000N9Z.jpg.

for the DIARETDB0, DIARETDB1 and DRIVE datasets [25], obtained 100% accuracy for each one, and outperforms the results of [24] for DIARETDB0 and DIARETDB1.

For e-ophtha-EX dataset, we obtained 98.78% accuracy, meaning that OD location failed only in one case. The reason why the method fails to detect OD on image DS000F4K.jpg (shown in Fig.18) is because the total optic disc region is not captured on the photograph, making that the pattern of the column wise pixel intensity variation profile could not be found. For a meaningful clinical diagnosis, it is necessary that the important landmarks such as optic disc, macula, fovea and vasculature can be clearly distinguishable in the fundus image, so in practice these types of fundus images are discarded and replaced for another retinal photographic capture of the same eye.

The obtained results show that the proposed method is robust and achieves high detection rate in the four compared databases. Distinctly, the results of the proposed approach were achieved without any alterations to the sizes of the input images or tested with a fraction of the images of the data set.

6. Conclusions and discussion

A new approach for the location of the OD in human retinal images was developed and presented. The approach results to be simple and reliable; especially for challenging images, including images with poor illumination, pathological changes, with dark OD due to uneven illumination and low contrast, with partial OD section and images with bright exudates whose size and intensity are similar to OD. The robustness of the proposed technique is guaranteed by evaluating the method in four publicly-available datasets: DIARETDB1 [37], DIARETDB0 [38], e-ophtha-EX [39], and DRIVE [40] obtaining a disc detection success rate of 100%, 100%, 98.78% and 100% respectively.

Distinctly, since anatomical features calculated are relative to image's original resolution, the results of the proposed approach were achieved without any transformations to the sizes of the input images, making our detection algorithm scalable in terms of image resolution. Unlike most approaches, since no training was required for the classification stage, no additional datasets are needed for this task and the results are calculated using all images of the datasets.

The proposed algorithm was implemented using MATLAB R2017a version. Considering that OD could present similar characteristics with some signs of diabetic retinopathy, the proposed approach can be applied to remove the OD region before the detection of these signs, avoiding the possibility of erroneously classifying OD sections as pathology lesions in automated diabetic retinopathy (DR) screening.

A novel approach for OD location in retinal images based on high intensity information of best observed channel (Red or Green) combined with information from the main blood vessels was proposed. The method has four main stages: OD pixel region candidate generation, promising OD regions detection, promising candidate features extraction, and classification. Given that datasets have images with non-uniform illumination, regional intensity variations are found along the fundus image, this to overcome the well-known unreliable use of a global high intensity threshold to locate promising OD regions. That led us to use a window partitioning approach for the extraction of local OD candidate regions.

Recapitulating, the proposed approach consists of a top-down approach, from a group of high intensity local regions with coarse level features to finer features on extended regions with minimum requirements on size and intensity distribution, which form the most promising OD regions. A model for the column wise pixel intensity variation is proposed, and the features are defined according to the expected OD pattern on the column wise pixel intensity variation model: presence of a Left Lobe (LL), a Right Lobe (RL) and Vasculature (V) between them, and distances from LL to V and V to RL. Classification is done accordingly to the presence of the LL-V-RL pattern.

The proposed algorithm can be negatively affected if the retinal vasculature is not distinguishable, i.e. vessels belonging to the main arcades have low contrast or are quite difficult to observe. On the OD pixel region candidate generation stage, the inclusion of the OD true region as candidate depends on OD true region having a relevant local intensity with respect of another bright regions or artifacts that might be present on the windowed section of the image. Another source of error could be when the vertical vessels that emerge from the OD are either not present or exhibit a low contrast in comparison with other vertical vessels in other regions of the retina, this could lead to an incorrect OD classification. For the correct classification of OD candidate regions using the model for the column wise pixel intensity variations across the optic disc it is necessary that the majority of the actual OD region will be present on the analyzed fundus image.

Conflict of interest

None.

Acknowledgements

The authors would like to thank the founders of the publicly available databases. Laura Uribe-Valencia likes to thank to Consejo Nacional de Ciencia y Tecnología (CONACYT) for doctoral scholarship with CVU No. 493055.

References

[1] D. Marin, M.E. Gegundez-Arias, A. Suero, J.M. Bravo, Obtaining optic disc center and pixel region by automatic thresholding methods on morphologically processed fundus images, Comput. Methods Programs Biomed. 118 (2015) 173–185, http://dx.doi.org/10.1016/j.cmpb.2014.11.003.
[2] M. Ortega, M.G. Penedo, J. Rouco, N. Barreira, M.J. Carreira, Retinal verification using a feature points-based biometric pattern, EURASIP J. Adv. Signal Process. 2009 (2009) 1–13, http://dx.doi.org/10.1155/2009/235746.
[3] Y. Jiang, Blood vessel tracking in retinal images, in: Proceedings of Image and Vision Computing, 2007, pp. 126–131 http://digital.liby.waikato.ac.nz/conferences/ivcnz07/papers/ivcnz07-paper24.pdf.
[4] D. Youssef, N.H. Solouma, Accurate detection of blood vessels improves the detection of exudates in color fundus images, Comput. Methods Programs Biomed. 108 (2012) 1052–1061, http://dx.doi.org/10.1016/j.cmpb.2012.06.006.
[5] C. Köse, U. Şevik, C. Ikibaş, H. Erdöl, Simple methods for segmentation and measurement of diabetic retinopathy lesions in retinal fundus images, Comput. Methods Programs Biomed. 107 (2012) 274–293, http://dx.doi.org/10.1016/j.cmpb.2011.06.007.
[6] W.M.D.W. Zaki, M.A. Zulkifley, A. Hussain, W.H.W.A. Halim, N.B.A. Mustafa, L.S. Ting, Diabetic retinopathy assessment: towards an automated system, Biomed. Signal Process. Control 24 (2016) 72–82, http://dx.doi.org/10.1016/j.bspc.2015.09.011.
[7] L. Xiong, H. Li, An approach to locate optic disc in retinal images with pathological changes, Comput. Med. Imaging Graph. 47 (2016) 40–50, http://dx.doi.org/10.1016/j.compmedimag.2015.10.003.
[8] A. Soltani, T. Battikh, I. Jabri, N. Lakhoua, A new expert system based on fuzzy logic and image processing algorithms for early glaucoma diagnosis, Biomed. Signal Process. Control 40 (2018) 366–377, http://dx.doi.org/10.1016/j.bspc.2017.10.009.
[9] P.S. Mittapalli, G.B. Kande, Segmentation of optic disk and optic cup from digital fundus images for the assessment of glaucoma, Biomed. Signal Process. Control 24 (2016) 34–46, http://dx.doi.org/10.1016/j.bspc.2015.09.003.
[10] I.W.R.A. Abdel-Ghafar, T. Morris, T. Ritchings, Progress towards automated detection and characterisation of the optic disk in Glaucoma and diabetic retinopathy, Med. Inform. Internet Med. 32 (2007) 19–25.
[11] B.G. Meindert Niemeijer, Michael D. Abràmoff, Fast detection of the optic disc and Fovea in color fundus photographs, Med. Image Anal. 13 (2009) 859–870, http://dx.doi.org/10.1016/j.pestbp.2011.02.012.Investigations.
[12] S. Sekhar, F.E. Abd El-Samie, P. Yu, W. Al-Nuaimy, A.K. Nandi, Automated localization of retinal features, Appl. Opt. 50 (2011) 3064–3075, http://dx.doi.org/10.1364/AO.50.003064.
[13] R.J. Qureshi, L. Kovacs, B. Harangi, B. Nagy, T. Peto, A. Hajdu, Combining algorithms for automatic detection of optic disc and macula in fundus images, Comput. Vis. Image Underst. 116 (2012) 138–145, http://dx.doi.org/10.1016/j.cviu.2011.09.001.
[14] R. Kamble, M. Kokare, G. Deshmukh, F.A. Hussin, F. Mériaudeau, Localization of optic disc and fovea in retinal images using intensity based line scanning analysis, Comput. Biol. Med. 87 (2017) 382–396, http://dx.doi.org/10.1016/j.compbiomed.2017.04.016.
[15] K. Akyol, B. Şen, Ş. Bayir, Automatic detection of optic disc in retinal image by using keypoint detection, texture analysis, and visual dictionary techniques, Comput. Math. Methods Med. 2016 (2016) 1–10, http://dx.doi.org/10.1155/2016/6814791.
[16] A.V. Deshmukh, T.G. Patil, S.S. Patankar, J.V. Kulkarni, Features based classification of hard exudates in retinal images, 2015 International Conference on Advances in Computing, Communications and Informatics, ICACCI 2015 (2015) 1652–1655, http://dx.doi.org/10.1109/ICACCI.2015.7275850.
[17] C.A.G. Sergio Bonafonte Royo, Retinopatía Diabética, Elsevier España, 2006.
[18] K. Akita, H. Kuga, A computer method of understanding ocular fundus images, Pattern Recognit. 15 (1982) 431–443, http://dx.doi.org/10.1016/0031-3203(82)90022-X.
[19] A.M.N. Allam, A.A.H. Youssif, A.Z. Ghalwash, Automatic segmentation of optic disc in eye fundus images: a survey, Electron. Lett. Comput. Vis. Image Anal. 14 (2015) 1–20, http://dx.doi.org/10.5565/rev/elcvia.680.
[20] O. Faust, U.R. Acharya, E.Y.K. Ng, K.H. Ng, J.S. Suri, Algorithms for the automated detection of diabetic retinopathy using digital fundus images: a review, J. Med. Syst. 36 (2012) 145–157, http://dx.doi.org/10.1007/s10916-010-9454-7.
[21] J. Rahebi, F. Hardalac, A new approach to optic disc detection in human retinal images using the firefly algorithm, Med. Biol. Eng. Comput. 54 (2015) 453–461, http://dx.doi.org/10.1007/s11517-015-1330-7.
[22] X.-S. Yang, Firefly algorithm, in: Nature-Inspired Metaheuristics Algorithms 2nd ed., Luniver Press, Frome, 2010, pp. 81–89.
[23] M. Foracchia, E. Grisan, A. Ruggeri, Detection of optic disc in retinal images by means of a geometrical model of vessel structure, IEEE Trans. Med. Imaging 23 (2004) 1189–1195, http://dx.doi.org/10.1109/TMI.2004.829331.
[24] I. Soares, M. Castelo-Branco, A.M.G. Pinheiro, Optic Disc Localization in Retinal Images Based on Cumulative Sum Fields, IEEE J. Biomed. Health Inform. 20 (2016) 574–585, http://dx.doi.org/10.1109/JBHI.2015.2392712.
[25] X. Wu, B. Dai, W. Bu, Optic disc localization using directional models, Ieee Trans. Image Process. 25 (2016) 4433–4442, http://dx.doi.org/10.1109/TIP.2016.2590838.
[26] R. Panda, N.B. Puhan, G. Panda, Robust and accurate optic disk localization using vessel symmetry line measure in fundus images, Biocybern. Biomed. Eng. 37 (2017) 466–476, http://dx.doi.org/10.1016/j.bbe.2017.05.008.
[27] S. Roychowdhury, D.D. Koozekanani, S.N. Kuchinka, K.K. Parhi, Optic disc boundary and vessel origin segmentation of fundus images, IEEE J. Biomed. Health Inform. 20 (2016) 1562–1574, http://dx.doi.org/10.1109/JBHI.2015.2473159.
[28] C. Wang, D. Kaba, Y. Li, Level set segmentation of optic discs from retinal images, J. Med. Bioeng. 4 (2015) 213–220, http://dx.doi.org/10.12720/jomb.4.3.213-220.
[29] B. Harangi, A. Hajdu, Detection of the optic disc in fundus images by combining probability models, Comput. Biol. Med. 65 (2015) 10–24, http://dx.doi.org/10.1016/j.compbiomed.2015.07.002.
[30] a Basit, Optic disc detection and boundary extraction in retinal images, Appl. Opt. 54 (2015) 3440–3447, http://dx.doi.org/10.1364/AO.54.003440.
[31] S. Bharkad, Automatic segmentation of optic disk in retinal images, Biomed. Signal Process. Control 31 (2017) 483–498, http://dx.doi.org/10.1016/j.bspc.2016.09.009.
[32] L.C. Rodrigues, M. Marengoni, Segmentation of optic disc and blood vessels in retinal images using wavelets, mathematical morphology and Hessian-based

multi-scale filtering, Biomed. Signal Process. Control 36 (2017) 39–49, http://dx.doi.org/10.1016/j.bspc.2017.03.014.
[33] A. Chakravarty, J. Sivaswamy, Joint optic disc and cup boundary extraction from monocular fundus images, Comput. Methods Programs Biomed. 147 (2017) 51–61, http://dx.doi.org/10.1016/j.cmpb.2017.06.004.
[34] S.B. Sakchai, V. Nattapol, W. Akara, U.S. Bunyarit, Fine exudate detection using morphological approach, Int. J. Appl. Biomed. Eng. 1 (2010) 45–50.
[35] X. Ren, J. Malik, Learning a classification model for segmentation, Proceedings Ninth IEEE International Conference on Computer Vision. 1 vol. 1 (2003) 10–17, http://dx.doi.org/10.1109/ICCV.2003.1238308.
[36] S.S. Radhakrishna Achanta, Appu Shaji, Kevin Smith, Aurelien Lucchi, Pascal Fua, SLIC superpixels compared to state-of-the-Art superpixel methods, IEEE Trans. Pattern Mach. Intell. 34 (2012) 2274–2281, http://dx.doi.org/10.14890/minkennewseries.68.2_214.
[37] T. Kauppi, V. Kalesnykiene, J.-K. Kamarainen, L. Lensu, I. Sorri, A. Raninen, R. Voutilainen, H. Uusitalo, H. Kalviainen, J. Pietila, The DIARETDB1 diabetic retinopathy database and evaluation protocol, Procedings of the British Machine Vision Conference 2007 (2007) 61–65, http://dx.doi.org/10.5244/C.21.15.
[38] T. Kauppi, V. Kalesnykiene, J. Kamarainen, L. Lensu, I. Sorri, DIARETDB0 : Evaluation Database and Methodology for Diabetic Retinopathy Algorithms, Machine Vision and Pattern Recognition Research Group, Lappeenranta University of Technology, Finland, 2006, pp. 1–17, http://www.siue.edu/šumbaug/RetinalProjectPapers/Diabetic Retinopathy Image Database Information.pdf.
[39] E. Decencière, G. Cazuguel, X. Zhang, G. Thibault, J.C. Klein, F. Meyer, B. Marcotegui, G. Quellec, M. Lamard, R. Danno, D. Elie, P. Massin, Z. Viktor, A. Erginay, B. Laÿ, A. Chabouis, TeleOphta: machine learning and image processing methods for teleophthalmology, IRBM 34 (2013) 196–203, http://dx.doi.org/10.1016/j.irbm.2013.01.010.
[40] R. Bernardes, P. Serranho, C. Lobo, Digital ocular fundus imaging: a review, Ophthalmologica 226 (2011) 161–181, http://dx.doi.org/10.1159/000329597.